Paper
Int'l J. of Aeronautical & Space Sci. 17(4), 614–621 (2016)
DOI: http://dx.doi.org/10.5139/IJASS.2016.17.4.614

IJASS
International Journal of Aeronautical and Space Sciences

Efficient Measurement System to Investigate Micro-Doppler Signature of Ballistic Missile

In-O Choi* and Kyung-Tae Kim**

Department of Electrical Engineering, POSTECH, 77 Cheongam-ro, Nam-gu, Gyeongbuk, Pohang 37673, Republic of Korea

Joo-Ho Jung***

Unmanned Technology Research Center, Korea Advanced Institute of Science and Technology, Daehak-ro, Yuseong-gu, Daejeon 34141, Republic of Korea

Si-Ho Kim****

Agency for Defense Development, Yuseong-gu, Daejeon 34186, Republic of Korea

Sang-Hong Park*****

Department of Electronic Engineering, Pukyong National University, Yongso-ro 45, Nam-gu, Busan 48513, Republic of Korea

Abstract

Micro-Doppler (MD) shift caused by the micro-motion of a ballistic missile (BM) can be very useful to identify it. In this paper, the MD signatures of three scale-model BMs are investigated using a portable measurement system. The measurement system consists of an X-band 2-by-2 phase comparison mono-pulse radar, and a mechanical device that can impart controlled spinning and coning motions simultaneously to a model to yield the MD signature that replicates the characteristic of each target and the corresponding micro-motion. The coning motion determined the overall period of MD, and the spinning motion increased its amplitude. MD was also dependent on aspect angle. The designed system is portable, and can implement many micro-motions; it will contribute to analysis of MD in various situations.

Key words: Micro-Motion, Mono-Pulse, Range-Doppler Algorithm, Ballistic Missile, Micro-Doppler

1. Introduction

Ballistic missiles (BM) are fast projectiles with small radar cross section (RCS) that follow a ballistic trajectory. Defending against BMs is a vital task in warfare. The range estimated using the two-way time-delay between the radar and BM, and the Doppler shift caused by the velocity are widely used to intercept BMs [1, 2]. However, a BM warhead can be accompanied by decoys, so efficient methods to distinguish the warhead from the decoys are required.

One efficient way to distinguish the warhead from the decoys is to exploit the differences in their micro-motions. Representative micro-motion dynamics are spinning and coning, which form the micro-Doppler (MD) feature that facilitates warhead recognition [3, 4, 5]. A maneuvering warhead travels along the flight trajectory with inherent micro-motion dynamics, which can be regarded as a unique signature of the warhead.

Most previous research related to MD is based on simulation of a target composed of isotropic point scatterers; in this system, discrepancies between the real scattering mechanism and the point scatterer may lead to significant errors in recognition. Thus, MD analysis based on the measured data is required. Recent measurement systems

* Ph. D Student : inochoi@postech.ac.kr
** Associate Professor
*** Research Professor
**** Senior Researcher
***** Associate Professor, Corresponding Author: radar@pknu.ac.kr

Received: March 16, 2016 Revised: October 25, 2016 Accepted: November 1, 2016

http://ijass.org pISSN: 2093-274x eISSN: 2093-2480

use stepped-frequency waveform (SFW) radar to measure targets in an anechoic chamber [6, 7]. However, SFW requires compensation for inter-pulse phase errors [8], and the fixed motion equipment [4, 9], and the target must be portable so that its MD can be analyzed in various clutter environments. Furthermore, the rotation velocity of the target for micro-motion dynamics must also be increased to resemble that of a real target.

In this paper, we investigated the dynamic MD signatures of scale models of three missiles. We used an efficient X-band measurement system that can measure MD in various cluttered environments. The measurement system is composed of a dual-motor system for micro-motion dynamics, and an X-band 2-by-2 phase-comparison mono-pulse (PCMP) radar to receive reflected radar signals from four antennas. Measurement results conducted outside the anechoic chamber demonstrates the efficiency of the devised system by clearly representing the MD signature of each target.

2. Micro-Doppler Principle and Measurement System

2.1 Micro-Doppler principle of BM

Spinning and coning (Fig. 1) are rotations around an axis in a local coordinate (x, y, z). The axis of spinning is inside the target and the axis of coning is outside it.

We use the procedure introduced in [4, 10] to derive the principle of MD of BM because the procedure is very easy to understand and clearly explains MD of BM. The monostatic chirp radar signal used for the measurement system at fast time t is

$$s_0(t) = \exp\left(j2\pi \left(f_0 t + \frac{Bt^2}{2\tau} \right) \right) \times rect\left(\frac{t}{\tau} \right) \tag{1}$$

where f_0 is the start frequency, B is the bandwidth, τ is the pulse duration, and $rect(\cdot)$ = 1 over t-τ/2 ≤ t ≤ t+τ/2 and 0 otherwise.

The reflected signal from a BM with a micro-motion is sampled at pulse repetition period T_s and is given by

$$g(t,t_s) = \sum_{k=1}^{K} A_k \exp\left(j2\pi \left(f_0(t-\tau_k(t_s)) + \frac{B(t-\tau_k(t_s))^2}{2\tau} \right) \right) \times rect\left(\frac{t-\tau_k(t_s)}{\tau} \right) \tag{2}$$

where t_s is the slow time which is a multiple of T_s, K is the number of the scatterers that comprise the BM, A_k is the amplitude of scatterer k, and $\tau_k(t_s)$ is the two-way fast-time delay at t_s between the radar and k. Assuming that k located at (x_k, y_k) is observed at $\theta(t_s)$ in the x-y plane, $\tau_k(t_s)$ is given by [10]

$$\tau_k(t_s) = \frac{2}{c}\left(R(t_s) + x_k(t_s)\cos\theta(t_s) + y_k(t_s)\sin\theta(t_s) \right) \tag{3}$$

where $R(t_s)$ is the distance from the radar to the origin of the local coordinate, and c is the speed of the light.

Then high-resolution range profiles (RPs) can be obtained by matched-filtering $g(t, t_s)$ by (1) in the t domain [11]. Because this operation is time-consuming, it is conducted in the fast-time frequency domain f; the resultant signal is

$$S_M(f,t_s) = \sum_{k=1}^{K} A_k \exp\left(-j2\pi f \tau_k(t_s) \right) \tag{4}$$

If $R(t_s)$ is removed by subtracting the known range to the target, and $P_k(t_s)$ is defined as $x_k(t_s)\cos\theta(t_s)$ + $y_k(t_s)\sin\theta(t_s)$, then $S_M(f, t_s)$ in the f domain can be inverse Fourier-transformed to

$$\begin{aligned} S_M(t,t_s) &= \int_{f_0}^{f_0+B} S_M(f,t_s)\exp(j2\pi ft)\,df \\ &= \sum_{k=1}^{K} A_k B \,\mathrm{sinc}\left(\pi B\left(t - \frac{2}{c}P_k(t_s) \right) \right) \exp\left(j\pi B\left(t - \frac{2}{c}P_k(t_s) \right) \right) \end{aligned} \tag{5}$$

Then by selecting the radar signal in range bin = ct/2 that contains the target, and differentiating the complex signal with respect to t_s, the time-varying Doppler frequency can be obtained as

$$f_D(t_s) = -\frac{B}{2}\frac{dP(t_s)}{dt_s} \tag{6}$$

Because P(t_s) depends on the time-varying micro-motion of BM, the number of

useful features that can be extracted increases after MD is represented in the time-frequency domain. In this paper, we represent MD by using the spectrogram (SP) given by

$$SP\left[x(t_s) \right](t_d, f_s) = \int_{-\infty}^{\infty} x(t_s) w(t_s - t_d) \exp(-j2\pi f t_s)\,dt_s \tag{7}$$

where $w(\cdot)$ is a window function.

MD variation of a BM that is spinning and coning can be modeled by a rotation matrix formed by Rodrigues' rotation formula [12]. Assuming that a vector $\bar{v}$ is rotated by θ around an axis $\bar{k}_e = (k_1, k_2, k_3)$, the rotated vector $\bar{v}_{rot}$ is expressed by

$$\bar{v}_{rot} = (I\cos\theta + [\bar{k}_e]_x \sin\theta + (1-\cos\theta)\bar{k}_e\bar{k}_e^T)\bar{v} = \mathbf{M}\bar{v} \tag{8}$$

where

$$\left[\bar{k} \right]_x = \begin{bmatrix} 0 & -k_3 & k_2 \\ k_2 & 0 & -k_1 \\ -k_2 & k_1 & 0 \end{bmatrix} \tag{9}$$

Similarly, for a scatter engaged in spinning and coning

motion starting from $\vec{p}_0$, the position at t_s is a product of two matrices

$$\vec{p}_t = \mathbf{M_c}(t_s)\mathbf{M_s}(t_s)\vec{p}_0 \tag{10}$$

where $\mathbf{M_c}$ and $\mathbf{M_s}$ are the rotation matrix constructed using the coning velocity vector and the spinning velocity vector, respectively (Fig. 1; Eq. 8). As a result, MD of the BM is given by

$$MD = \frac{2}{\lambda}\left[\frac{d(\mathbf{M_c}\mathbf{M_s})}{dt_s}\vec{p}_0\right]\bullet\vec{a}_R = \frac{2}{\lambda}\left[\left(\frac{d\mathbf{M_c}}{dt_s}\mathbf{M_s} + \mathbf{M_c}\frac{d\mathbf{M_s}}{dt_s}\right)\vec{r}_0\right]\bullet\vec{a}_R \tag{11}$$

where $\vec{a}_R$ is the unit vector of the radar line of sight, λ is the wavelength, and $\bullet$ is the inner-product operator. MD is the combination of the spinning and the coning frequencies due to the multiplication of the elements in the coning and the spinning matrices.

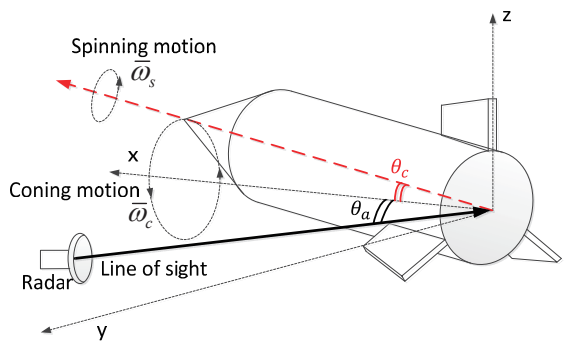

Fig. 1. Micro-motion dynamics of BM.

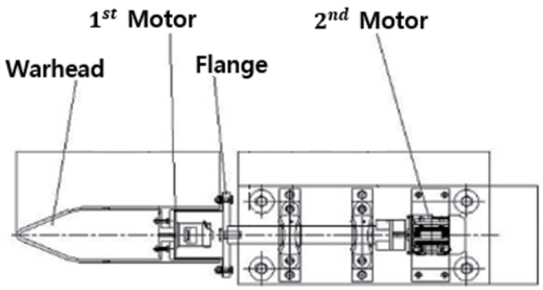

(a) Micro-motion device

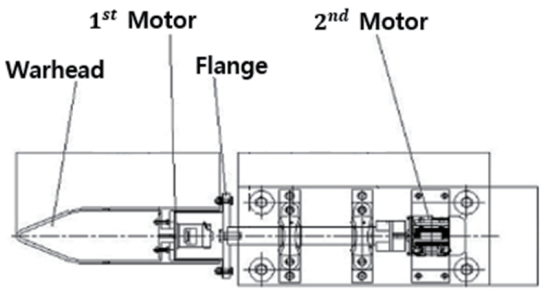

(b) Flanges for coning angle

Fig. 2. Schematic of the micro-motion device.

2.2 Measurement system

To simulate the micro-motion of BM, we designed a dual-structure motor system. composed of two inverter motors, one inside the missile and one outside it (Figs. 2, 3). The motor inside the missile is impart the spinning motion of the missile and the second motor imparts coning motion (Figs. 2a, 3a). The coning angle can be adjusted by changing the flange that connects the first and the second motors (Fig. 2b). To simulate the effect of various coning angles, the flange was designed to have tilt angles ranging from 0° to 15° in increments of 1°. Each motor can be operated up to 500 RPM by adjusting a knob in the control box (Fig. 3b) that controls the current flow in the inverter. Therefore, combined use of the two motors and the flanges can yield micro-motions with various spinning and coning velocities at various coning angles.

For the measured target, three scale models were designed. Each was made of aluminum with 3-mm thickness to represent the perfect inducting characteristic of the missile while minimizing the weight (Fig. 4). In addition, each target has a unique size of warhead and body, and number of wings. Model 1 (Fig. 4a) was manufactured to study the general MD signature of BM. Models 2 (Fig. 4b) and 3 (Fig. 4c) were to study the effect of spinning in general missiles such as cruise missiles. The whole system was supported by a steel frame that can be assembled. The second motor was covered with

(a) Micro-motion device

(b) Control box

Fig. 3. Manufactured micro-motion device.

DOI: http://dx.doi.org/10.5139/IJASS.2016.17.4.614

radar-absorbing material to eliminate any effects of motor rotation (Fig. 5).

A portable X-band 2-by-2 radar system was designed to obtain the radar signal (Fig. 6, Table 1). The transmitter emits an up-chirp signal in which the frequency increases linearly. The reflected electromagnetic signal is sequentially received by the four-channel antenna receivers (Fig. 6a). The four signals are synchronized, then joined as a single complex signal by using a single-pole four-through (SP4T) switch. The trigger signal for synchronization between analogue to digital converter (ADC) and arbitrary waveform generator (AWG) is generalized by an Atmega 128 micro-processor. This processor also forms antenna selection signals for the control of the SP4T switch. The micro-processor is controlled by a host computer and an RS-232 (Fig. 6b).

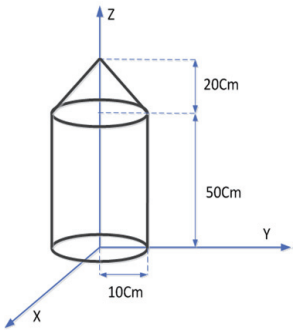

(a) Model 1

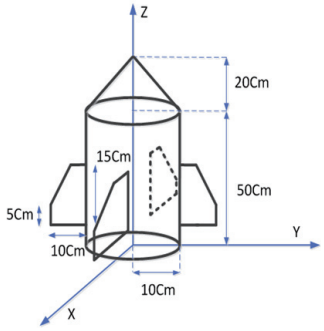

(b) Model 2

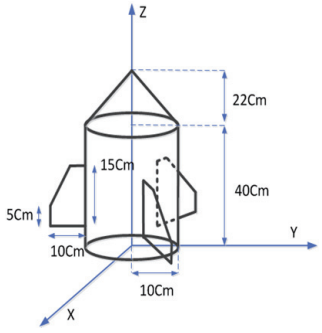

(c) Model 3

Fig. 4. Diagrams of the models used for micro-Doppler extraction and measurement.

2.3 Signal processing procedure

To demonstrate the operation of the designed measurement system, 4,096 pulses were received from a missile-shaped target with pulse repetition frequency = 1,000 Hz, and 4096 RPs were obtained by performing matched-

Fig. 5. Measurement setup. To eliminate the effect of micro-motion of the second motor, it is covered with radar-absorbing material.

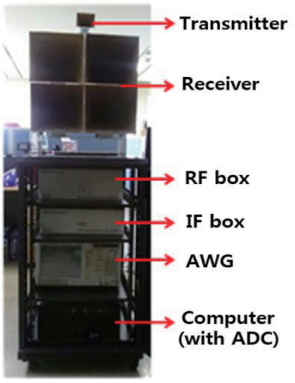

(a) Radar

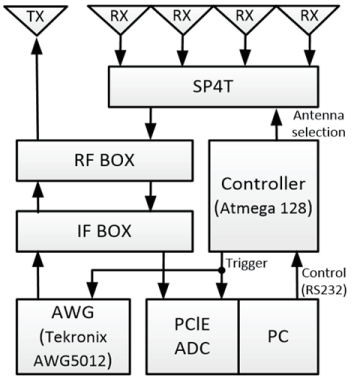

(b) Block diagram

Fig. 6. Measurement radar and block diagram.

filtering using the stored replica of the transmitted signal in (1). Then, the range bin containing the target, i.e., bt, was selected by finding the range bin with the maximum energy of the signal projected onto the fast time domain, and the signal st in this bin was obtained. Because the noise and clutter can distort the MD signal, s_t was digitally band-passed using a rectangular bandpass filter (BPF) in the frequency domain. Finally, (7) was used to transform the band-passed signal s_{bpf} to the time-frequency domain, and residual noise was removed by thresholding (Fig. 7).

3. Experimental Results

3.1 Experimental result of system verification

An experiment was performed to verify the overall operation of the designed system by using Model 2 engaged in micro-motion with arbitrary parameters in a wide-open hall of the LG building of Pohang University of Science Technology. After matched filtering, 4096 RPs were obtained with the target located at range bin b_t = 250 (Fig. 8a). The radar signal s_t varied over time due to the micro-motion of

Table 1. Specification of the radar

Specification	Value
Carrier frequency	10 GHz
Transmission power	29.8 dBm (max)
Frequency range	40 - 60 MHz
Sampling bits	14 bits
Sampling frequency	65 MHz
Dynamic range	83 dB
Transmission antenna	Gain: 15 dB Beam width: 30°
Reception antenna	Gain: 20 dB Beam width: 20°

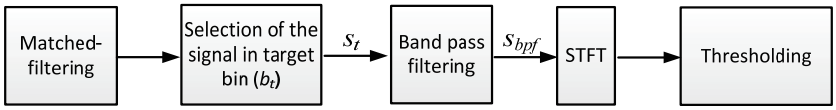

Fig. 7. Signal processing procedure

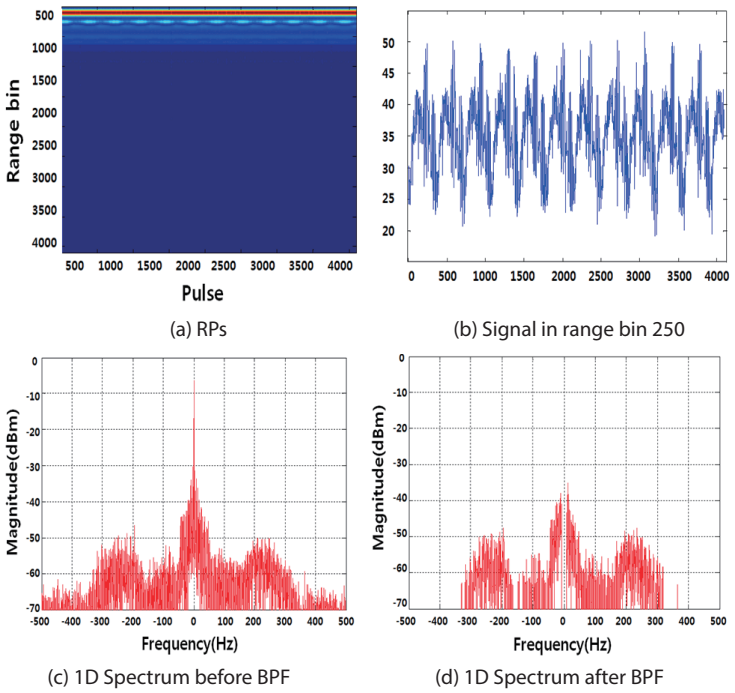

Fig. 8. Measurement result.

DOI: http://dx.doi.org/10.5139/IJASS.2016.17.4.614

the target (Fig. 8b). The one-dimensional (1D) frequency spectrum obtained by Fourier transformation shows that most of the MD signal falls in the frequency range -330 ≤ f ≤ 330 Hz with the largest energy at 0 Hz (Fig. 8c). Thus, frequency components outside this range and the zero frequency were eliminated digitally (Fig. 8d).

In forming the spectrogram of s_{bpf}, for the sake of clarity the pixel with the largest value was set to 0 dB and those smaller than -10 dB were set to -10 dB. The spectrogram (Fig. 9) of the MD signal after time-frequency transform clearly represents the micro-motion of the target. Due to the coning motion of the main body composed of a cylinder and a cone, sinusoidal MD motion occurred at -50 ≤ f ≤ 50 Hz. Because of the time-varying nature of the radar cross-section (RCS) of the tilted cone and the cylinder, the amplitude of coning motion in spectrogram was time-varying. Furthermore, micro-motion caused by a combination of coning and spinning of the three wings clearly appeared at -200 ≤ f ≤ 300 Hz and 200 ≤ f ≤ 300 Hz. Close examination of these ranges shows that MD of the three wings are represented by two or three vertical lines that arise periodically due to the sharp variation in the RCS of a plate.

3.2 Analysis of MD spectrogram

Effects of motion parameters were analyzed to demonstrate the accuracy of the designed system. The angular velocity ω_s of spinning was set to 10.5 rad/s = 100 RPM or 15.7 rad/s = 150 RPM, and the angular velocity ω_c of coning was set in the same manner. Two coning angles θ_c = 7 and 15° were used to study the effect of coning angle. Aspect angle θ_a was varied between 0 and 90° to determine its effect on MD (Table 2).

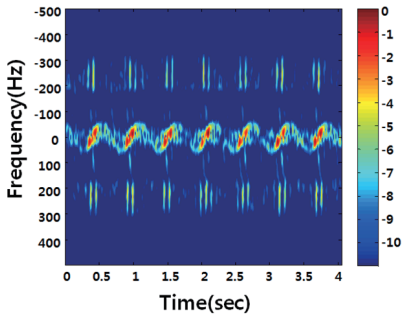

Fig. 9. MD image after BPF

Table 2. Motion and observation parameters

Motion	Value
Spinning motion (rad/s)	10.5, 15.7
Coning motion (rad/s)	10.5, 15.7
Coning angle	7°, 15°
Aspect angle	0° - 90°

MD images (Fig. 10) of Model 1 rotating at ω_c = 15.7 rad/s with θ_c = 15° and observed at θ_a = 90° clearly represent the coning motion. MD of the body repeats every 0.4 s which corresponds to the coning frequency f_c = 2.5 Hz. The range of MD is different from the ideal values due to the small RCS of the nose; the ideal maximum Doppler frequency f_{max} of the nose tip drawing a circle with a radius = 0.7tan(15°) = 0.19 m is 196.4 Hz and this is not seen in the MD image, whereas f_{max} = 100 Hz that corresponds to a 0.36-cm cylinder is seen.

MD images (Fig. 11) of Model 2 rotating at ω_c = ω_s = 15.7 rad/s with θ_c = 15° represents the addition of spinning and coning frequencies. As proved in (11), the spinning MD of the three wings at θ_a = 90° was added to and subtracted from the coning MD, yielding f_{max} = 426.3 Hz, which is very close to

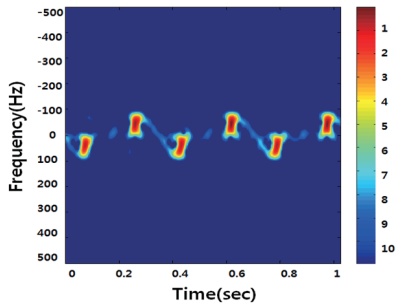

Fig. 10. MD image of model 1 (ω_c = 15.7 rad/s, θ_c = 15°, θ_a = 90°).

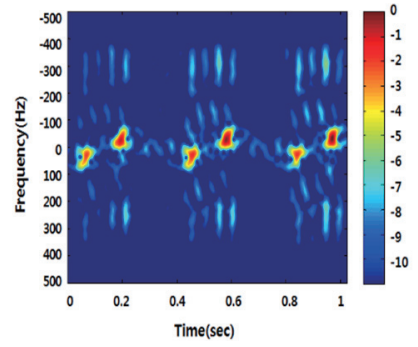

(a) θ_a = 90°

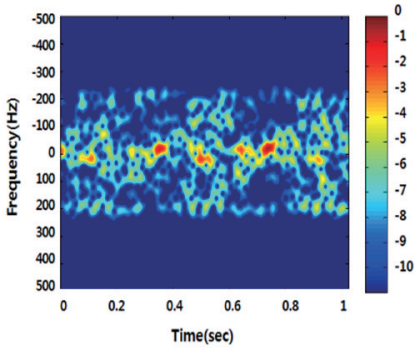

(b) θ_a = 60°

Fig. 11. MD image of model 2 (ω_s = ω_c = 15.7 rad/s, θ_c = 15°).

the ideal value (Fig. 11a). In addition, four wings are clearly represented by four vertical lines that repeat at f_c = 2.5 Hz. Comparison of MD images obtained at θ_a = 90° (Fig. 11a) and 60° (Fig. 11b) shows the angular dependency; ideal f_{max} = 366.6 Hz because the velocity was scaled by cos(30°) = 0.86, but measured f_{max} = 230 Hz due to the small RCS of the wing tip.

MD images (Fig. 12) of Model 3 obtained at θ_a = 90° and θ_c = 15° for four combinations of (ω_s, ω_c) demonstrate the effect of each component. Comparison of MD images for (10.5, 10.5) Hz and (10.5, 15.7) Hz proves that fc determines the repetition of the MD image of the target (Figs. 12a, b); MD in Fig. 12a repeats at f_c = 1.67 Hz whereas that in Fig. 12b repeats at f_c = 2.5 Hz. Comparison of MD images for (10.5, 10.5) Hz and (15.7, 10.5) Hz shows that the spinning MD adds the additional frequency (Figs. 12a, c) of approximately 50 Hz due to the increased spinning frequency. Comparison of Fig. 12b and d shows the same result.

Finally, the effect of the coning angle was studied by comparing MD images of Model 3 with θ_c = 7° and 15°, observed at ω_s = ω_c = 15.7 rad/s, θ_a = 90° (Fig. 13). Although the MD repeated with the same period, MD image was very dependent on θ_c; the amplitude of the main body was much larger at θ_c = 15° than at θ_c = 7° (Fig. 13). In addition, the location of the MD of each blade changed due to RCS variation of the three wings, yielding totally different MD images.

4. Conclusion

In this paper, the dynamic MD signatures of BM were

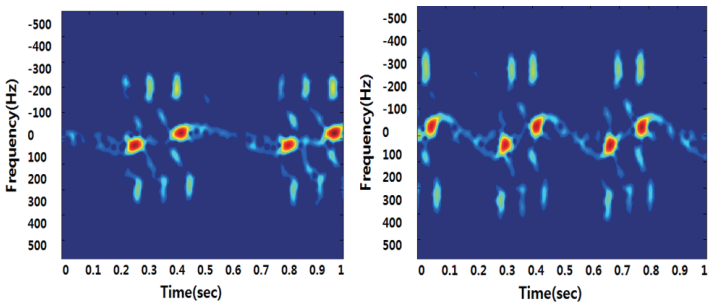

(a) (10.5, 10.5) (b) (10.5, 15.7)

(c) (15.7, 10.5) (d) (15.7, 15.7)

Fig. 12. MD image of model 3 for (ω_s, ω_c) (θ_c = 15°, θ_a = 85°).\

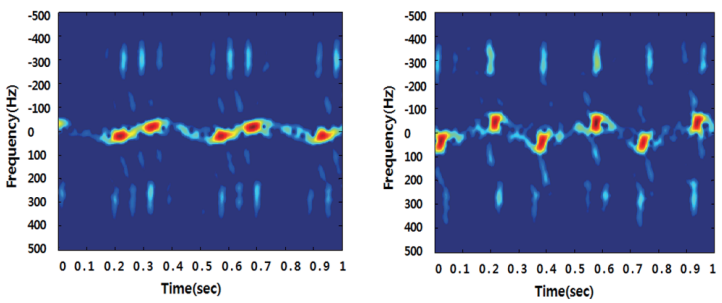

(a) 7.5° (b) 15.0°

Fig. 13. MD image of model 3 for two θ_c values (ω_s = ω_c = 15.7 rad/s, θ_a = 90°).

DOI: http://dx.doi.org/10.5139/IJASS.2016.17.4.614

investigated using a portable micro-motion device, three scale models, and a portable X-band measurement system. The micro-motion device implemented spinning and coning motions of the scale models, and the designed radar system composed of the dual motor system and the X-band 2-by-2 PCMP radar successfully measured the MD signal. MD signals were represented as spectrograms after matched-filtering, selection of b_v, and BPF. Analysis of MD signature showed that the coning motion determined the overall period of MD, and that the spinning motion increased its amplitude. MD was very dependent on the aspect angle because of the angular dependency of RCS of the models.

MD can occur in various types of targets engaged in micro-motion and these targets may exist in various environments that can produce various clutter signals. Because the designed system can be moved to any environments and many of such micro-motions can be implemented by the designed motion-device, it will contribute to successful analysis of the MD signal in various situations

Acknowledgement

This work was supported by the Sensor Target Recognition Laboratory (STRL) program of the Defense Acquisition Program Administration and the Agency for Defense Development.

References

[1] Hale, F. J., *Introduction to Space Flight*, Prentice Hall, 1993.

[2] Lemnios, W. Z. and Grometstein, A. A., "Overview of the Lincoln Laboratory Ballistic Missile Defense Program", *Lincoln Laboratory Journal*, Vol. 13, 2002, pp. 9-32.

[3] Chen, V., *The Micro-Doppler Effect in Radar*, Artech House, 2011.

[4] Gao, H., Xie, L., Wen, S. and Kuang, Y., "Micro-Doppler Signature Extraction from Ballistic Target with Micro-Motions", *IEEE Transactions on Aerospace Electron Systems*, Vol. 46, Issue. 4, 2010, pp. 1969-1982.

[5] Sun, H. X. and Liu, Z., "Micro-Doppler Feature Extraction for Ballistic Missile Warhead", *IEEE International Conference on Information and Automation*, 2008, pp. 1333-1336.

[6] Levanon, N., *Radar Signals*, Wiley-IEEE Press, 2004.

[7] Fukushima, C. and Hamada, N., "A Study on Stepped Frequency Radar by Using Intra-Pulse Coded Modulation", *Proceedings of The World Congress on Engineering and Computer Science*, 2008, pp. 391-396.

[8] Park, S. H., Kim, H. T. and Kim, K. T., "Improved Autofocusing of Stepped-Frequency ISAR Images Using New form of Particle Swarm Optimization", *Electronics Letters*, Vol. 45, Issue. 20, 2009, pp. 1053-1055.

[9] Pan, X., Wang, W., Liu, J., Feng, D., Liu, Y. and Wang, G., "Features Extraction of Rotationally Symmetric Ballistic Targets Based on Micro-Doppler", *Progress In Electromagnetics Research*, Vol. 137, 2013, pp. 727-470.

[10] Jung, J. H., Kim, K. T., Kim, S. H. and Park, S. H., "An Efficient ISAR Imaging Method for Multiple Targets", *Progress In Electromagnetics Researc*h, Vol. 146, 2014, pp. 133-142.

[11] Mahafza, B. R., *Radar Systems Analysis and Design Using MATLAB*, CRC Press, 2013.

[12] Murray, R. M., Li, Z, and Sastry, S. S., *A Mathematical Introduction to Robotic Manipulation*, CRC Press, 1994.